Reduced modeling of crash barriers for design optimization of space frame automobile structures

M. Tischer, E.J. Wehrle, H. Baier
Lehrstuhl für Leichtbau, Technische Universität München

Abstract

In this work, a simplified model has been developed for the Euro NCAP offset deformable barrier suitable for use in the optimization of space frame automobile structures. The model improves the prediction accuracy of discrete structures and components without a force-distributing vehicle body shell, by restricting unrealistic local deformation of the barrier. It also drastically reduces the computational effort compared to the shell and solid barrier models typically used. In order to develop this simplified model, investigations are carried out using the standard and well tested barrier models provided by LSTC. The developed model then was verified by simulation with a rigid impactor, full-vehicle models and also body–in-white models. It is shown that the simplified barrier allows a direct investigation of body-in-white or space frame structures without making a great compromise in respect of the simulation quality. This enables the consideration of the Euro NCAP offset deformable barrier in optimization and helps to identify robust designs in an early development phase.

Keywords

Reduced modeling, Offset deformable barrier, Euro NCAP, design optimization

1 Introduction

Structural design optimization has advanced from its origin in linear elastostatic problems to highly nonlinear, transient problems of crashworthiness [1]. Nonlinear finite-element analysis with explicit time integration requires high computational effort, therefore, restricting the scope of design optimization. This is especially the case when considering impact load cases with deformable barriers. The standard, complex shell and solid models occupy a significant portion of total simulation time.

Further in the preliminary design phase, often discrete structures like body-in-white (BiW) or crash boxes are used due to lower the calculation time and to reduce the modeling effort of parameterized models. These are needed for parameter studies or optimization. It uses the fact, that only a small amount of parts is directly relevant to structural responses and energy absorption [2].

During impact, the kinetic energy E_V^{kin} of the vehicle is mainly transformed by deformation into internal energy of the barrier E_B^{int} and the internal energy of the vehicle E_V^{int} (eq. 1).

$$E_V^{kin^{t=t_0}} = E_V^{int} + E_B^{int} + E_V^{kin^{t=t_{end}}} \qquad (1)$$

The internal energy of the barrier is a product of the crush force F_b and the crush length s (eq.2).

$$E_B^{int} = \int_{s_0=0}^{s_1=s} F_b \cdot ds \qquad (2)$$

Due to the equilibrium of forces, the crush force F_b and the reaction force applied to the vehicle F_v are equal (eq. 3).

$$F_b = F_v = m_v \cdot a_v \qquad (3)$$

The crush force and the energy absorbed by the deformable barrier strongly depend on the surface size of the impacting vehicle (impactor). When a full-vehicle model hits a deformable barrier, the front part crushes (fig. 1) and, therefore, distributes the forces to the underlying structures. The impacting surface is set by the vehicle size. During a parameter study or optimization of discrete structures this surface is significantly smaller without the body shell. In addition during the variation of model parameter like the bumper height, the impacting area is also changing. This can cause the structure to intrude deeply into the barrier and, thereby, produce a structural response, which is not reasonable to the actual load case (fig. 2a). Here the barrier absorbs an unrealistically small amount of energy. Especially, when a structure is optimized using such a load case the results can lead to a useless design.

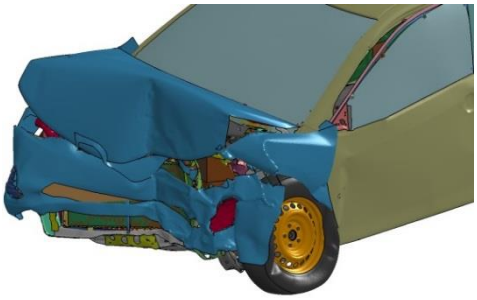

Fig. 1: Vehicle front after impact

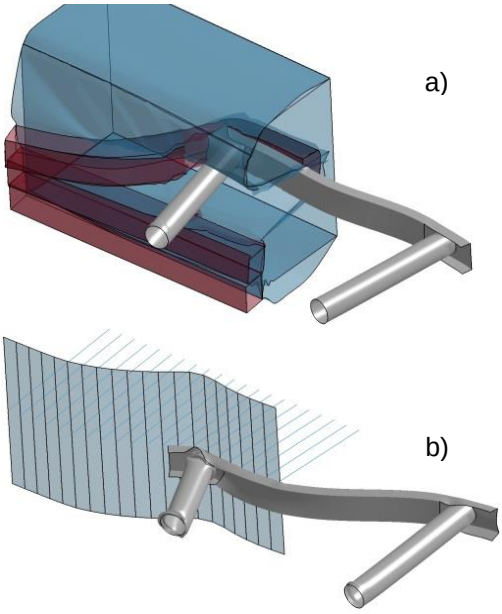

Fig. 2: Comparison of a front crash system against solid ODB (a) and simplified barrier model (b) 32 ms after impact

The aim is to develop a simplified model for the Euro NCAP offset deformable barrier (ODB) [3] in order to reduce the computational effort. The model should also improve the prediction accuracy of discrete structures and components without a force-distributing vehicle body shell, by restricting unrealistic local deformation of the barrier (fig. 2b, bottom).

2 Study of the behavior of Euro NCAP ODB models

The ODB (fig. 3) is designed to represent the characteristics of a vehicle front end. The barrier consists mainly of two parts, the main block and the bumper. Either are made of thin aluminum foil honeycombs with an anisotropic hexagon structure. The three-parted barrier bumper (1.74 MPa) is clearly stiffer than the main block (0.34 MPa). The bumper has an aluminum facing sheet and the main block is partly covered by an aluminum cladding sheet. Both sheets are glued to the honeycomb. The cladding sheet also connects the barrier bumper to the main block of the barrier.

In order to develop a simplified model of the barrier suitable for optimization, investigations are carried out using the standard and well tested barrier models provided by LSTC [4, 5]. The shell model[1] serves here as the reference model. In this model, the aluminum honeycomb structures of the bumper and the main block are modeled by over a million shell elements. Each side of the hexagons is represented by three elements. Due to this method, the model can actually show the characteristic buckling of the honeycomb. It is the most realistic representation of the real barrier, but due to the enormous amount of elements the calculation times are very high.

In addition, a simpler and less computational demanding solid model[2] is used. Here, the honeycomb structure is modeled with 41916 8-node solid elements and a honeycomb material model [6]. In this type of modeling the characteristic buckling in longitudinal direction is well represented by the compression of the elements. A realistic picture of the deformation transverse to the honeycomb structure is not feasible as well as the deformation of locally loaded structure. Nevertheless it is possible to validate force-deflection or acceleration curves of an impacting structure in a qualitative manner [7].

Apart from the modeling of honeycomb structure, both the shell- and the solid barrier models can simulate the rupture of the cladding sheets and the disconnection of the glued parts (bumper-main block, honeycomb-sheets).

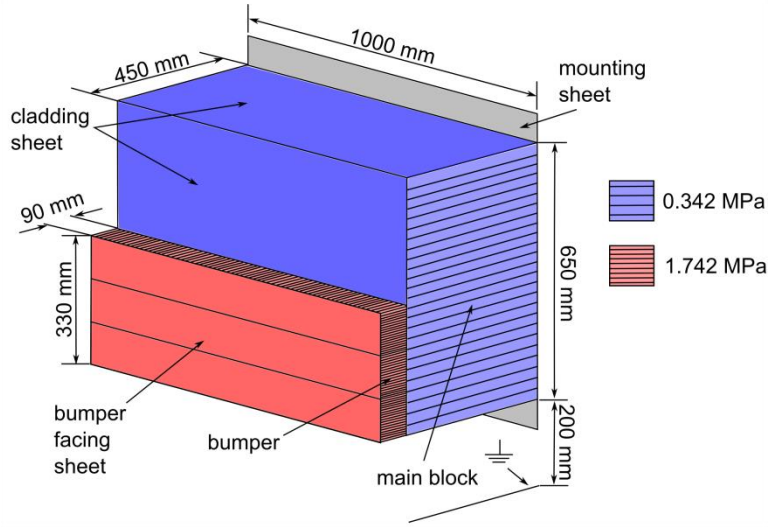

Fig. 3: Parts and measurements of Euro NCAP ODB

2.1 Analysis of general behavior

The first simulation is used for examining the general behavior of the barrier during an impact. The focus is on the interaction between the bumper and main block. A rigid impactor which has only one degree of freedom in direction of the shell barrier is covering the whole frontal area. The test setup is shown in fig. 5a. The impacting speed corresponds to the Euro NCAP test. The mass is adjusted so that the barrier is fully compressed during the impact. Fig. 4 shows the filtered and unfiltered force applied to the impactor as a function of intrusion. The filtering is in accordance to SAE J 211, which recommends the CFC60 class for the barrier face force.

The impact process is then divided into several phases, which are described in the following:

Phase 1:	The impactor hits the barrier. The force peak results from the initial contact and the honeycomb structure, which begins to buckle.
Phase 2:	Because of the much higher stiffness, the bumper firstly remains undeformed. The honeycomb structure of the main block behind the bumper is pressed reward and crushes (fig. 5b). The structure above is pulled down due to the the cladding sheet
Phase 3:	The main block above the bumper is hit and starts to buckle (fig. 5c).
Phase 4	The honeycomb of the main block folds, while the bumper is still intact.
Phase 5	The honeycomb structure of main block behind the bumper is compressed until the stiffness of the bumper is reached and the honeycomb of the bumper starts to fold.

[1] LSTC.ODB.Shell6pe.Shell model
[2] LSTC.ODB.Solid.Solid.02242009 model

Phase 6 The remaining honeycomb of bumper and main block buckles and the crushed structure starts to compress (fig. 5d).

Phase 7 The barrier compresses further. The force increases rapidly until the impactor starts to bounce back

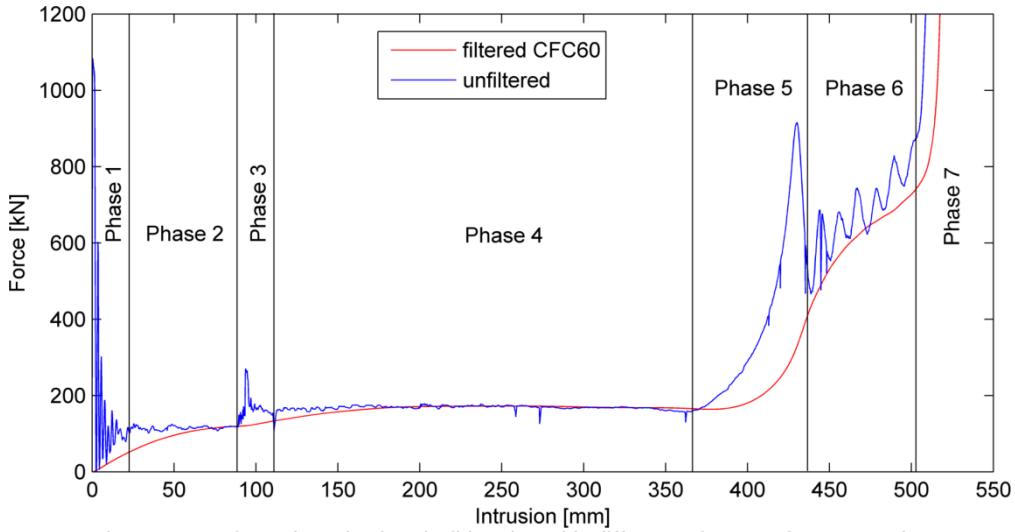

Fig. 4: Force-intrusion plot for shell barrier with different phases of compression

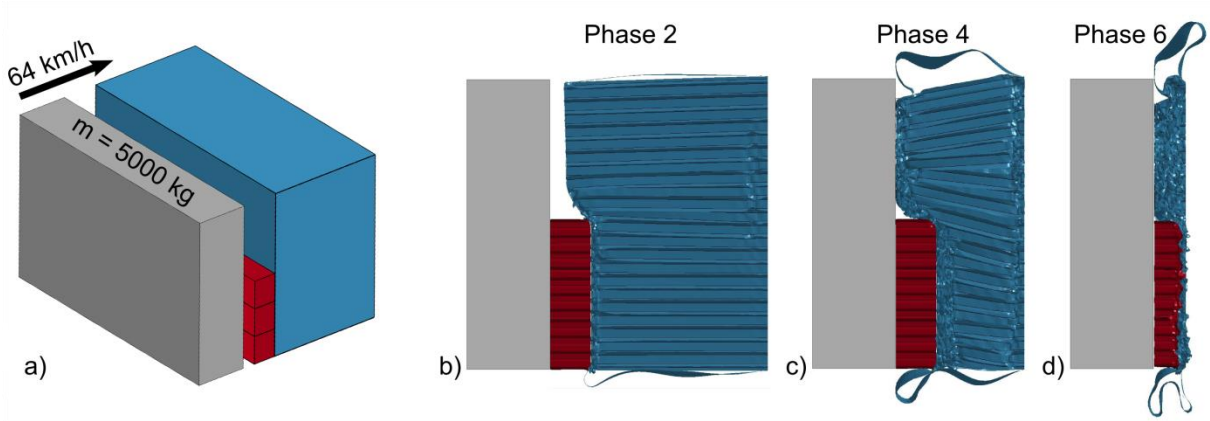

Fig. 5: Simulation setup for rigid impactor (a) in phase 2 (b), phase 4 (c) and phase 6 (c) of compression process

2.2 Analysis of width dependency of the impactor

The crash behavior of impactors of full barrier height but different widths is simulated. The position and the degree of overlap is shown in fig. 6. All degrees of freedom of the impactors are locked except in direction of the barrier. The layout is based on how a vehicle with increasing width would hit the barrier according to the Euro NCAP protocol. Fig. 8 shows the force-intrusion relationship in dependence to the degree of overlap. From 0 to 400mm the force distributing effect of the bumper and the cladding sheets can be seen. This effect leads to higher force levels, because honeycomb beside the impactor is also crushed. Above 400 mm there is nearly a linear relationship between the impactor width and the distributed force by the barrier. Fig. 9 shows the results for the solid barrier. Here the effect of crushed honeycombs beside the impacting area is clearly larger and the force levels are in total higher than the force levels simulated by the shell barrier. Fig. 7 shows the deformation of the solid barrier after 18 ms with an impactor of 50% overlap. It can been seen how the honeycomb beside the impactor is activated.

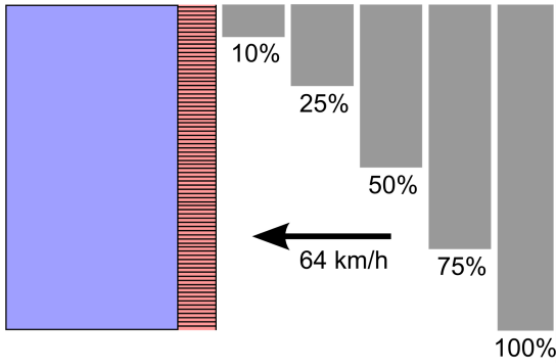

Fig. 6: Simulation setup for width dependency test (top view)

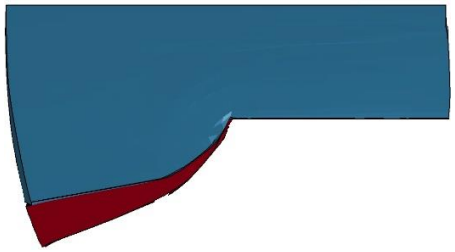

Fig. 7: Deformation of 50% impactor against solid barrier after 20ms (top view)

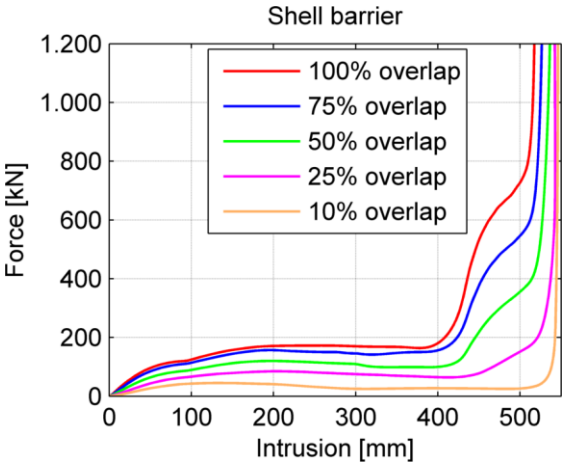

Fig. 8 Force-Intrusion plot dependent to impact width of shell barrier model (CFC60)

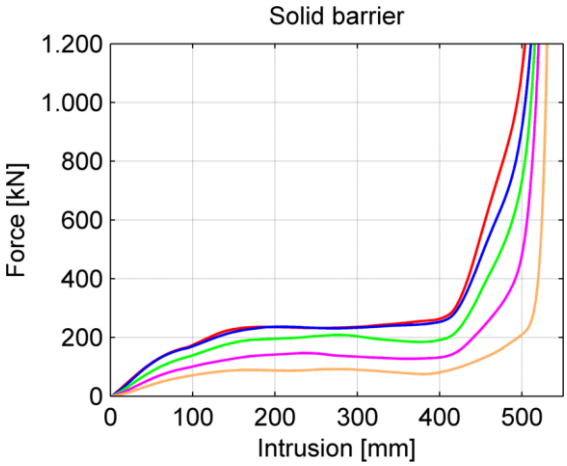

Fig. 9: Force-Intrusion plot dependent to impact width of solid barrier model (CFC60)

2.3 Analysis of height dependency of the impactor

Analog to the width dependency, the influence of the impactors height is tested. Now they have the full width of the barrier, but different heights. Fig. 10 is showing the sizes of the impactors and their position in relation to the barrier. The resulting forces for shell- and solid barrier are shown in fig. 12 and 13. The effect of additionally crushed honeycombs next to the impacting area is much higher than in the previous width dependency test. This is caused by the bumper and the cladding sheet. From 0 mm to 100 mm of intrusion, the resulting forces are nearly identical for all impactors. Above that, the 75% and 100% impactors (solid model even 50%) show the same resulting forces. All three parts of the bumper maintain connection by the adhesive bond to the cladding sheet. Only exception is the 10% impactor against the solid barrier, where the cladding sheet rips apart and therefore only a small part of the main block is crushed (fig. 11).

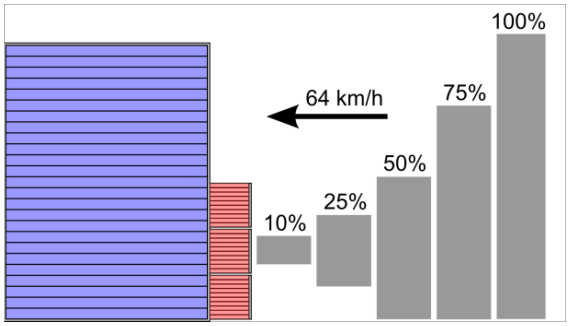

Fig. 10: Simulation setup for height dependency test (side view)

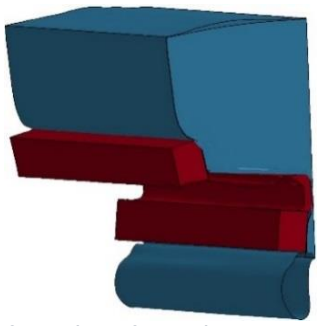

Fig. 11: Deformation of 10% impactor against solid barrier after 18ms

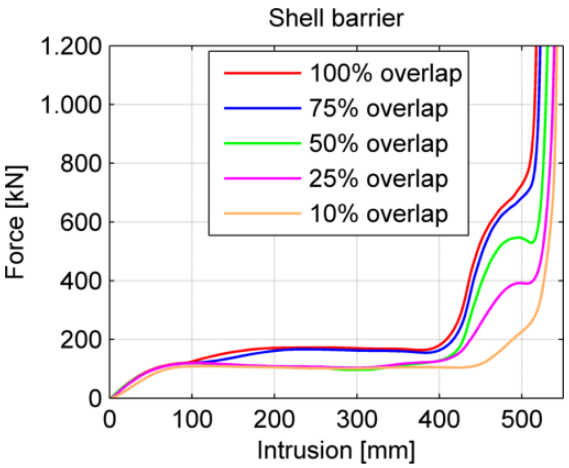

Fig. 12: Force-Intrusion plot dependent to impact height of shell barrier model (CFC60)

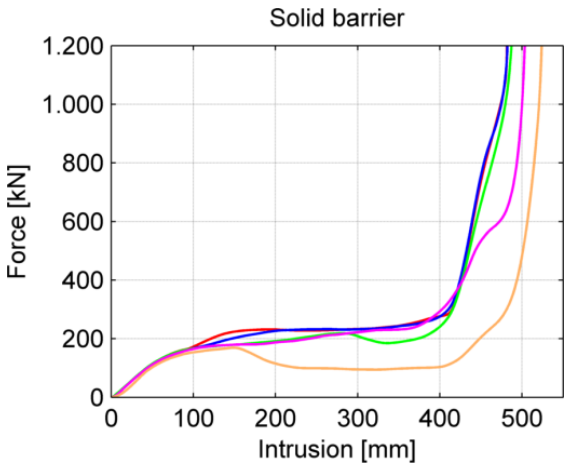

Fig. 13: Force-Intrusion plot dependent to impact height of solid barrier model (CFC60)

2.4 Simplified barrier model

Based on the results of the height and width dependence tests, a simplified barrier model is derived suitable for vehicles or vehicle substructures of different sizes and masses. Fig. 14 shows the FEM model and a schematic representation of the simplified barrier.

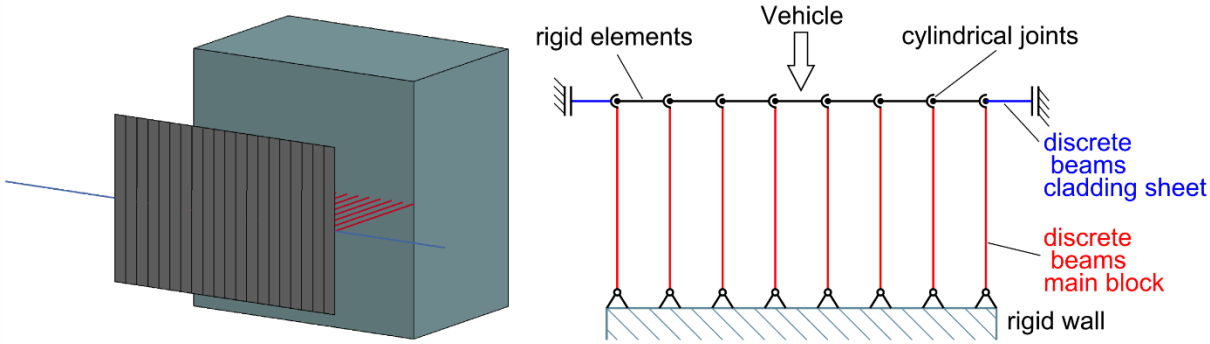

Fig. 14: FEM model (left) and schematic representation of the simplified barrier (right)

In the model, the energy absorbing main block and bumper are represented by 21 nonlinear discrete beams. The force displacement curve of these beams is derived from the force-intrusion relationship of the 100% overlap test of the shell barrier (fig. 4). The beam element nodes at the backside are locked in all degrees of freedom.

The frontal element nodes are mounted to rigid elements, which represent the cladding sheet of the barrier. These rigid elements prevent the local intrusion of discrete impacting structures. This based on the assumption that an outer skin deforms to a closed force distributing surface. The results of the height dependency test showed no significant difference between 75% and 100% overlap (fig. 12 and fig. 13). This is the case for a motor hood height about 680mm or higher, which should be appropriate for most classes of cars.

Though to ensure a certain flexibility, the area of the modeled cladding sheet is divided in to 20 vertical stripes connected by hinge joints. The up and downward movement of all nodes of the barrier is prevented by constraints. Additionally the front cladding sheet is hung laterally by nonlinear discrete beams. This hanging of the barrier prevents it from losing lateral stability.

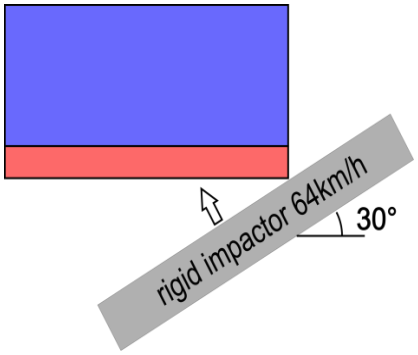

Fig. 15: Simulation setup for calibration of discrete nonlinear beams cladding of cladding sheet

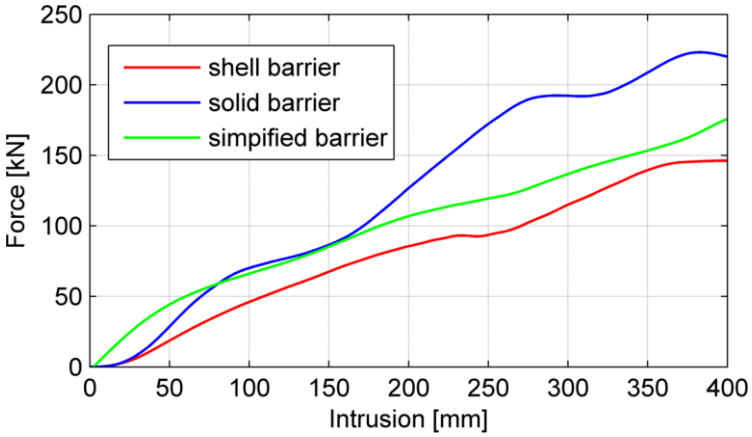

Fig. 16: Force-Intrusion comparison of a 30°impactor (CFC60)

To calibrate the force displacement curve of the important laterally beams, a simulation with a 30° impactor (fig. 15) is accomplished. This test represents a worst case scenario as due to the Euro NCAP protocol in general there are not such lateral speeds. Fig. 16 shows the results of the calibrated simplified barrier model in comparison to the shell and solid. The impactor can only intrude up to 400mm until it hits the upper right corner of the rigid block the barrier is mounted on. The simulated forces are normal to the impact front face.

To complete the calibration, the previously conducted width and height dependency tests are also performed with the new simplified barrier. Fig. 17 shows the force-intrusion relationship in dependence to impact width. The separation of the force levels of the different impactors is comparable to the solid barrier model. The amount of force lies between the shell and solid barrier models depending on the impactors width. As expected the simplified barrier model shows no dependence to impact height (fig. 18), which is part of the concept.

A comparison of the basic specifications of the shell and solid barrier models as well as the simplified model can be seen in tab. 1. It shows the drastic speed-up of the developed barrier.

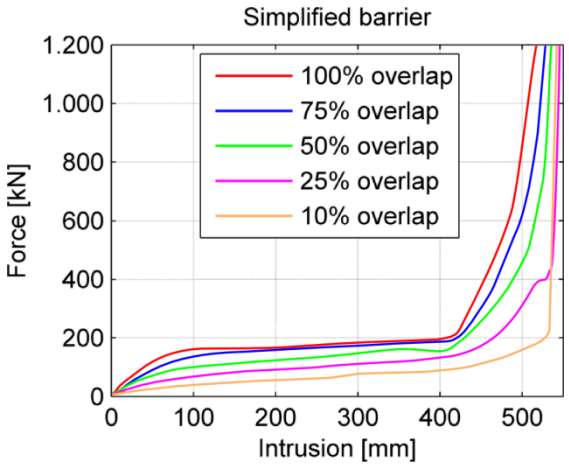

Fig. 17: Force-Intrusion plot dependent to impact width of simplified barrier model (CFC60)

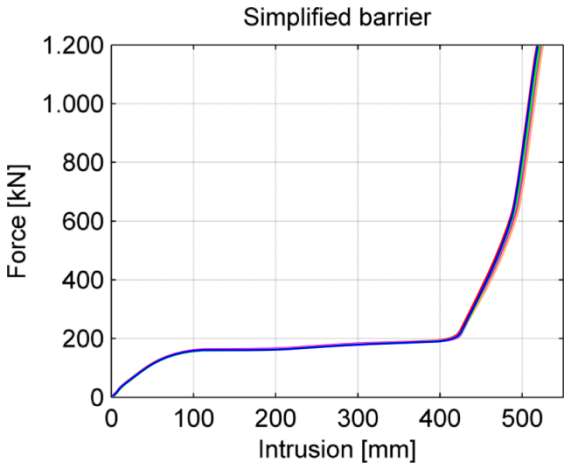

Fig. 18: Force-Intrusion plot dependent to impact height of simplified barrier model (CFC60)

	LSTC shell barrier	LSTC solid barrier	simplified model
Nodes	1 085 806	71 103	1643
Beam elements	0	0	21
Shell elements	1 504 793	22 203	1040
Solid elements	0	41 916	0
Element sum	1 504 793	64 119	1067
Calculation time*	28 h 7 min	16 min 46 s	34 s

*Table 1: Comparison shell, solid and simplified barrier model *(Intel Xeon E5-2637 v2)*

3 Verification of the simplified barrier model

For verification, the simplified barrier model is compared to the shell and solid barriers. Two vehicle models are used as an impactor: Vehicle 1 based on a Toyota Yaris and Vehicle 2 based on a Toyota Camry[3]. Vehicle 2 is about 100 mm wider and 30% heavier than Vehicle 1. The simulation setup matches the Euro NCAP frontal crash against a deformable barrier with 40% offset. A comparison of the crash behavior of both FEM models to the actual cars can be found in [8] and [9]. Additionally a BiW model of each vehicle was created to proof the concept of the simplified barrier. Here all parts unimportant for the structural responses are removed (fig. 19). The mass of the removed parts is added to the main structure via mass lumping.

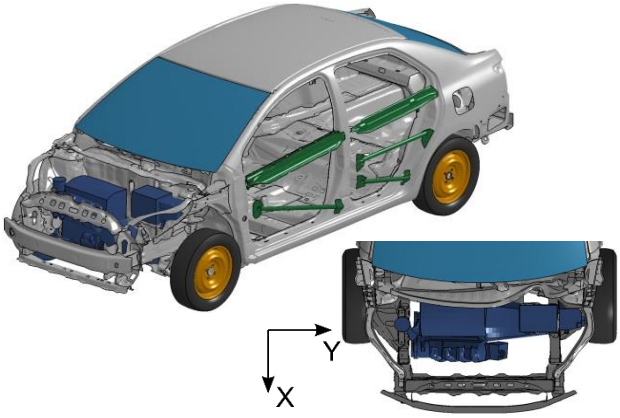

Fig. 19: BiW model and detailed top view of BiW front part Vehicle 1

Accelerations in x- and y-direction ($\ddot{u}_x$, $\ddot{u}_y$) are measured with seatbelt accelerometers at the center of gravity (CoG) as well as the velocities in x- and y-direction. Passenger dummy models are not considered to reduce the computational effort and instead the occupant loading criteria (OLC) $\ddot{u}_{OLC}$ [10] is used. All simulated acceleration and velocity data is filtered in accordance to SAE J 211 with CFC60 and CFC180. To further evaluate the simplified barrier model, the vehicle deformations and the areas with effective plastic strain after impact are compared as well as the total, kinetic and internal energy for all simulations. The internal energy directly corresponds to absorbed energy by the vehicle structure and the barrier.

3.1 Comparison, results and benefits of the simplified barrier model

Fig. 20 and 21 are showing the accelerations at CoG in x-direction for Vehicle 1 and 2. Considering the nature of crash pulses, the structural responses of the simplified barrier are in good agreement with those of the LSTC standard shell and solid barriers. Due to the force distributing effect of the simplified barrier, the BiW models show no substantial difference to the full models. The same applies to the acceleration in y-direction for Vehicle 2 (fig. 23), with a minor except for the BiW model, which is explained later. The acceleration of Vehicle 1 (fig. 22) oscillates, but the mean acceleration and the magnitude are comparable. The difference between both vehicles in the general shape of the curves in y-direction results from the fact, that the data of Vehicle 1 is plotted in a local coordinate system and Vehicle 2 in a global one.

The velocities at CoG in x- and y-direction for are shown in fig. 24 to 27. All recorded velocity data matches pretty well for the different barriers against Vehicle 1 and 2 including the BiW model.

[3] This model has been developed by The National Crash Analysis Center (NCAC) of The George Washington University under a contract with the FHWA and NHTSA of the US DOT (*http://www.ncac.gwu.edu)*

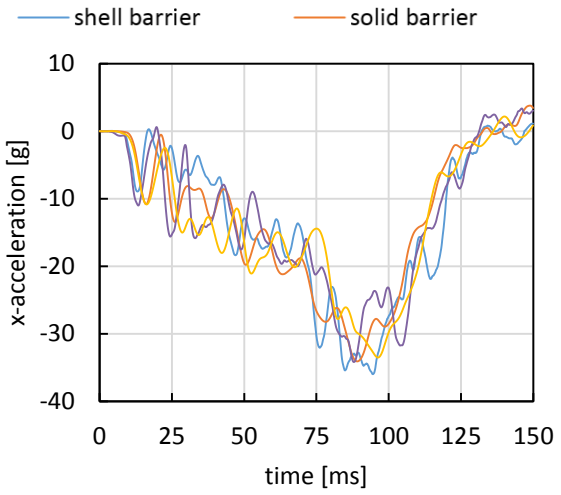

Fig. 20: Acceleration at CoG in x-direction Vehicle 1 (CFC60)

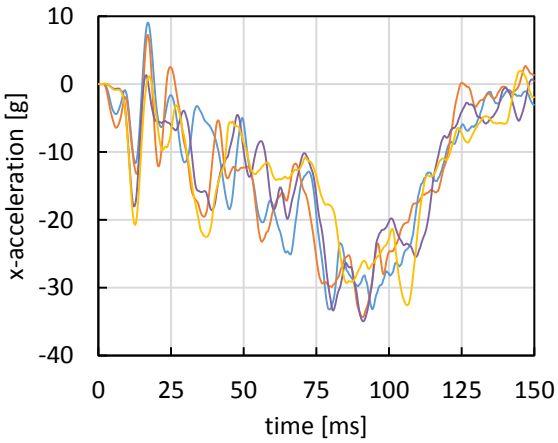

Fig. 21: Acceleration at CoG in x-direction Vehicle 2 (CFC60)

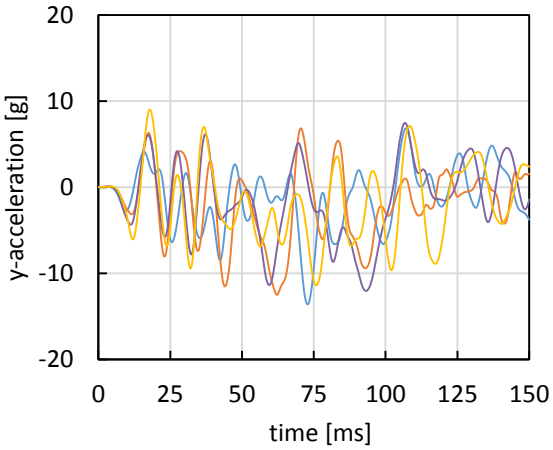

Fig. 22: Acceleration at CoG in y-direction Vehicle 1 (CFC60)

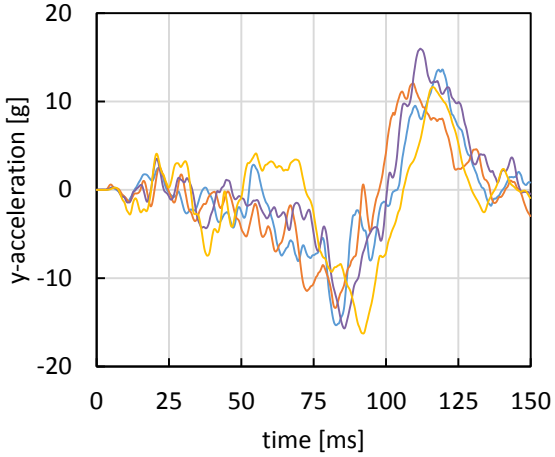

Fig. 23: Acceleration at CoG in y-direction Vehicle 2 (CFC60)

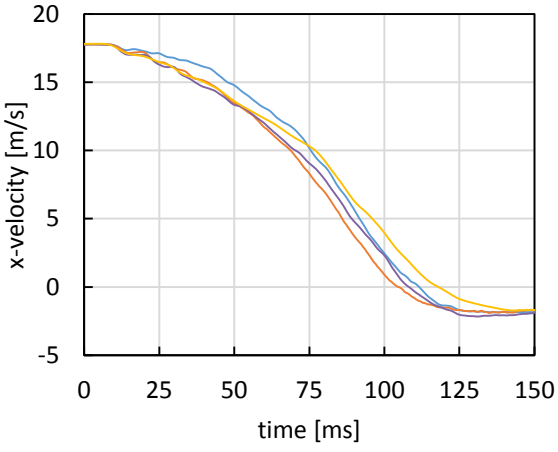

Fig. 24: Velocity at CoG in x-direction Vehicle 1 (CFC180)

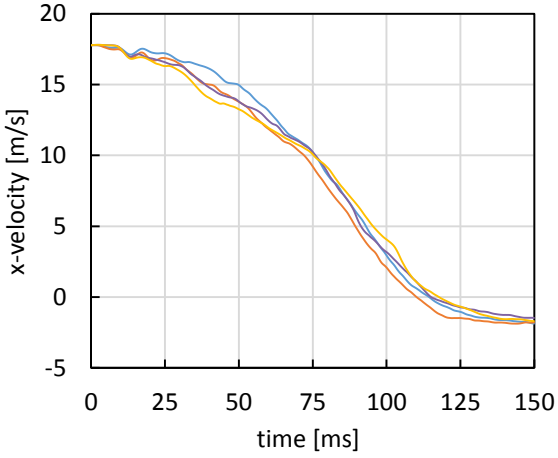

Fig. 25: Velocity at CoG in x-direction Vehicle 2 (CFC180)

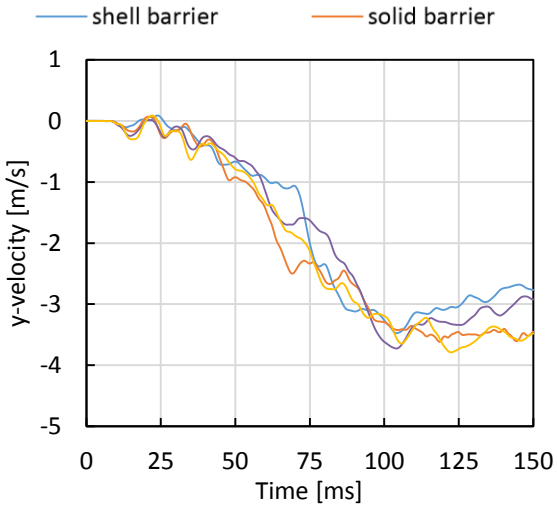

Fig. 26: Velocity at CoG in y-direction Vehicle 1 (CFC180)

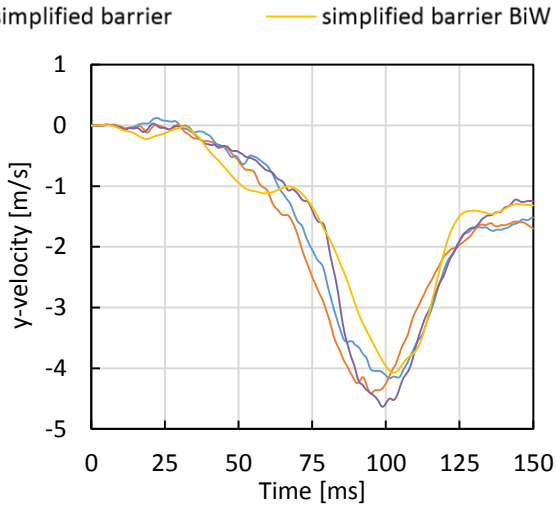

Fig. 27: Velocity at CoG in y-direction Vehicle 2 (CFC180)

The deformations after 150 ms of the main structure are very close for Vehicle 1 including the BiW model (fig. 28). The size and the position of areas with effective plastic strain are comparable. This is also the case for Vehicle 2 (fig. 29). Here all three barrier models show nearly the same level of deformation and effective plastic strain with the full vehicle model. Although the results of the BiW model are similar, the simple substitution model for the missing door is too weak. This leads to more deformation on the impacting driver side than the full model. With a better modelling off the door, the results should be clearly improved.

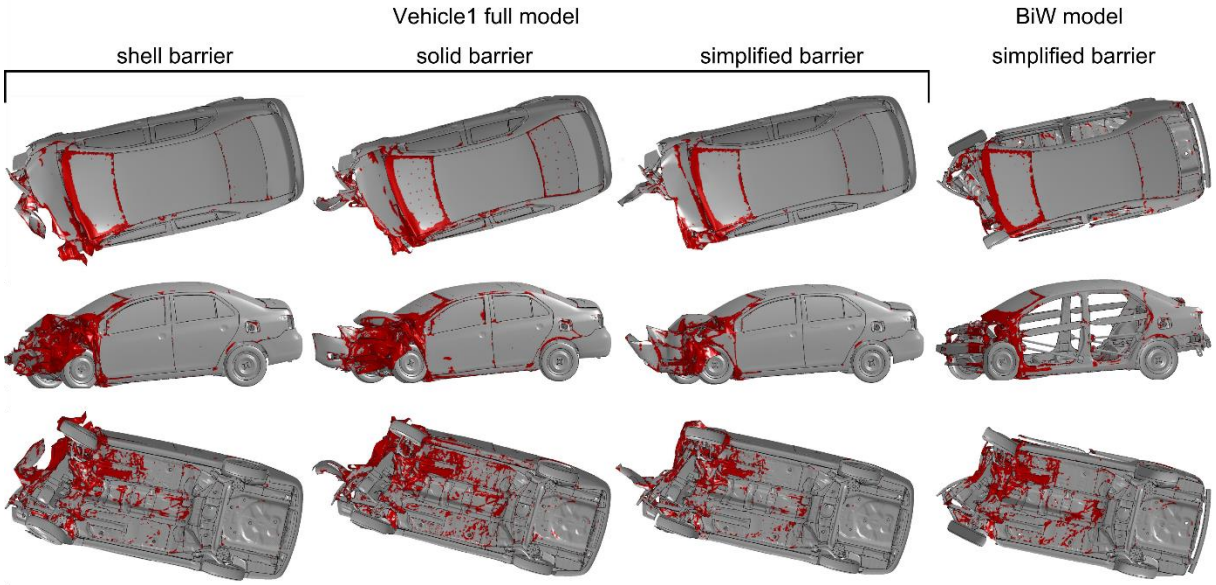

Fig. 28: Vehicle 1 comparison of final deformation and plastic strain (red) for full and BiW model of against shell, solid and simplified barrier model (barriers are hidden)

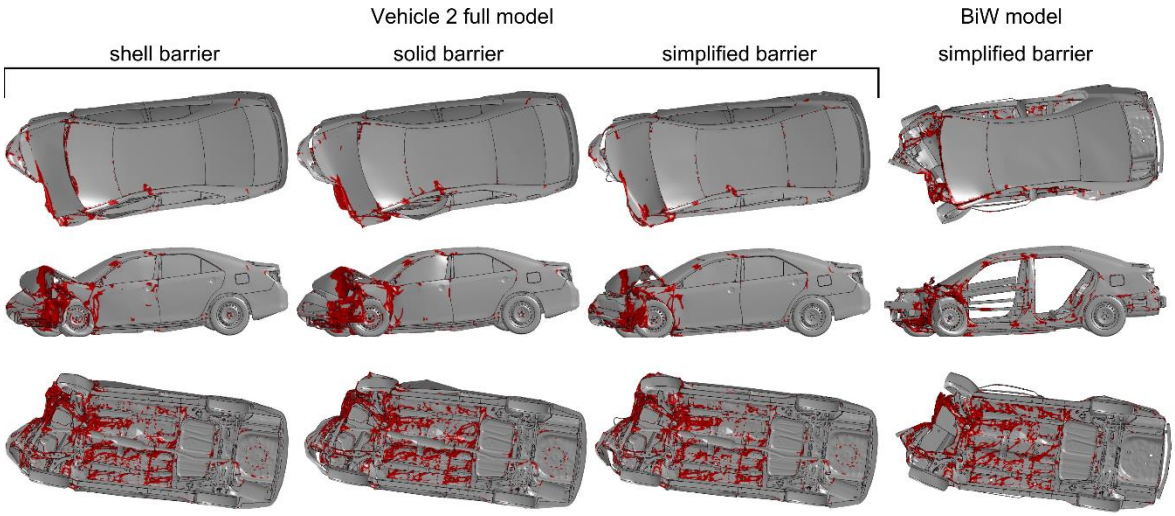

Fig. 29: Vehicle 2 comparison of final deformation and plastic strain (red) for full and BiW model of against shell, solid and simplified barrier model (barriers are hidden)

Fig. 30 and 31 are showing the total, kinetic and internal energies during the simulations of Vehicle 1 and Vehicle 2. The total energies remain constant and proof that no external work occurred. It can be seen how the kinetic energy is transformed into internal energy. The curves for the shell barrier show a slightly lower initial deceleration, because the shell representation of honeycomb allows for more local deformation than the solid and simplified barriers. This is also observed in the width dependency test, where the effects of additionally crushed honeycombs are less pronounced. The differences between the simplified barrier and the solid barrier are very low, even the simulations with the BiW model. The difference between the sum of the kinetic and internal energy to the total energy due to some sliding energy and hourglass energy in the vehicle and shell barrier models.

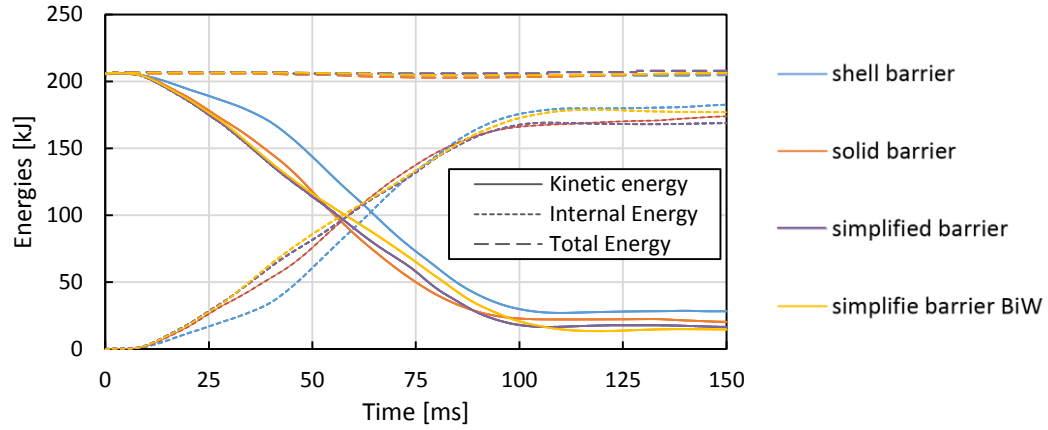

Fig. 30: Vehicle 1 comparison of total, kinetic, and internal energy for full and BiW model against shell, solid and simplified barrier model

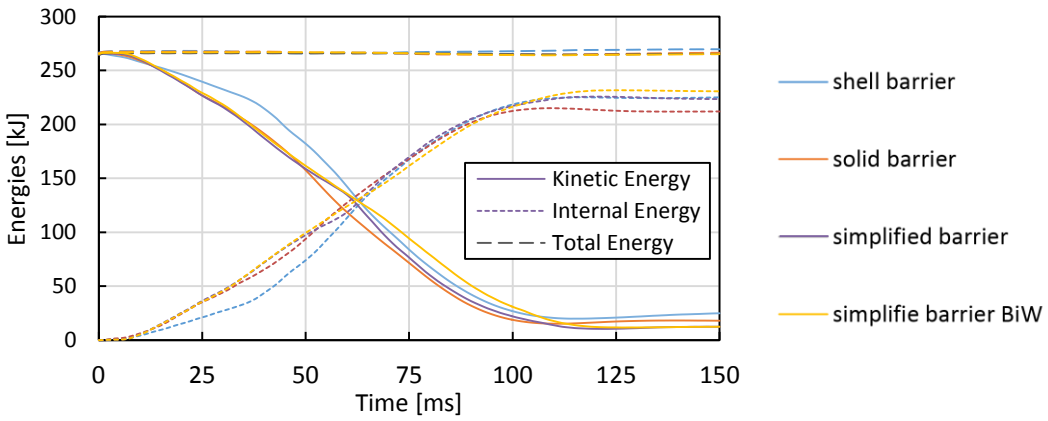

Fig. 31: Vehicle 2 comparison of total, kinetic, and internal energy for full and BiW model against shell, solid and simplified barrier model

Vehicle model		Full model			BiW model
Barrier model		Shell model	Volume model	Simplified model	Simplified model
Vehicle 1	max $\lvert\ddot{u}_x\rvert$	35.9 g	34.1 g	34.2 g	33.5 g
	max $\lvert\ddot{u}_y\rvert$	13.6 g	12.5 g	12.0 g	11.7 g
	$\ddot{u}_{OLC}$	36.7 g	38.1 g	36.2 g	37.7 g
Vehicle 2	max $\lvert\ddot{u}_x\rvert$	33.2 g	34.3 g	35.0 g	32.6 g
	max $\lvert\ddot{u}_y\rvert$	15.3 g	13.4 g	15.7 g	16.3 g
	$\ddot{u}_{OLC}$	36.2 g	35.9 g	36.1 g	36.7 g

Table 2: Comparison max. $\ddot{u}_x$ and $\ddot{u}_y$ at CoG, OLC

Finally a comparison of the maximum acceleration pulses, the OLCs and computation times for both vehicles (tab. 2). It shows the low variation of the maximum pulses, especially the OLC where the maximum difference is about 5%.

4 Summary

A new simplified FE model of the Euro NCAP offset deformable barrier has been developed and verified by simulation with a rigid impactor, full-vehicle models, and BiW models. Special focus is given to the computational afford of the barrier and the possibility of direct investigation of vehicle structures without force distributing skin. The new simplified barrier is based on the results of different parameter studies of the standard LSTC shell and solid barriers.

Computational speed-ups of the new model range from 2 to more than 15, while showing good agreement with LSTC standard shell and solid element barriers. It is shown that the simplified barrier enables a direct investigation of BiW or space frame structures without making a great compromise in respect of the simulation quality. The advantage lies not only in the lower calculation times, effort is also reduced to model a vehicle structure suitable for crash simulation against a deformable barrier. BiW and space frame models can be used without using the outer skin.

This enables the consideration of the Euro NCAP ODB in optimization and helps to identify robust designs in an early phase of development.

5 Literature

[1] Duddeck F., *Multidisciplinary optimization of car bodies.* Structural and Multidisciplinary Optimization 35, pp. 375-389, 2008

[2] Volz K. H. ,*Physikalisch begründete Ersatzmodelle für die Crashoptimierung von Karosseriestrukturen in frühen Projektphasen*. Dissertation, Technische Universität München, 2011

[3] *Frontal impact testing protocol* –Version 6.0. Euro NCAP, 2012

[4] Bala S., Bhalsod D., *Recent Developments on LSTC Barriers Models,* 9. LS-DYNA Anwenderforum, Bamberg, 2010

[5] Mehrdad, H. S., *In Investigation to Compare the Application of Shell and Solid Element Honeycomb Model in ODB*, 7. European LS-DYNA User's Conference, 2009

[6] LS-DYNA Theory Manual, 2011

[7] Fellner B., Jost T, *Layout, Validation and Benchmark of an all new Frontal Offset Barrier FEM Model*, 7. European LS-DYNA User's Conference, 2009.

[8] *Development & Validation of a Finite Element Model for the 2010 Toyota Yaris Passenger Sedan*, Technical Report, The George Washington University, 2011

[9] NCAC, *Toyota Camry Finite Element Model Version 1*. Technical Report, The George Washington University, 2014

[10] Kübler L., Gargallo S., Elsäßer K: *Bewertungskriterien zur Auslegung von Insassenschutzsystemen,* ATZ Automobiltechnische Zeitschrift, 111, pp. 426-433., 2009